International Journal of Fatigue 84 (2016) 28–39

Contents lists available at ScienceDirect

International Journal of Fatigue

journal homepage: www.elsevier.com/locate/ijfatigue

Role of nanotwins on fatigue crack growth resistance – Experiments and theory

Sertan Alkan [a], Piyas Chowdhury [a], Huseyin Sehitoglu [a,*], Richard G. Rateick [b], Hans J. Maier [c]

[a] Department of Mechanical Science and Engineering, University of Illinois at Urbana-Champaign, 1206 W. Green St., Urbana, IL 61801, USA
[b] Honeywell Aerospace, 3520 Westmoor St., South Bend, IN 46628, USA
[c] Institut fur Werkstoffkunde, Leibniz Universität Hannover, D-30823 Garbsen, Germany

ARTICLE INFO

Article history:
Received 11 September 2015
Received in revised form 6 November 2015
Accepted 13 November 2015
Available online 21 November 2015

Keywords:
Damage tolerance
Nanoscale twin
Threshold stress intensity
Microstructure
Residual dislocation

ABSTRACT

The study of near-threshold fatigue crack growth has long remained an empirical field due principally to the highly microstructure-sensitive nature thereof. The primary challenges have been to forward physical model(s) informed by the governing micromechanism(s), which would be able to predict the experimental behaviors devoid of empiricism. Today, we have sophisticated experimental techniques (e.g. digital image correlation, electron microscopy) as well as atomistic simulation tools (e.g. molecular dynamics) at our disposal to finally revisit the century old fatigue problem in the light of physical phenomena therein. This paper is geared towards achieving such a feat with a very special type of materials, nano-twinned alloys, as the candidate materials, which are of great recent interest due to their reportedly superior damage properties. Specifically, we investigate how the microstructural features (e.g. slip transfer mechanism at coherent twin boundaries, twin thickness/spacing, frictional stress, pre-existent near-tip slip density) can be modulated to improve the damage resistance. The results suggest that these parameters considerably affect the crack propagation impedance (as quantified in terms of $\Delta K_{\text{eff}}^{th}$). A thorough discussion of the current findings and the most recent literature developments in this regard are provided.

1. Introduction

1.1. Motivation and objective

Nanotwinned metals and alloys are novel emerging materials that are drawing considerable research interests thanks to their superior mechanical properties [1–3]. Given their considerable promise, their fracture and fatigue properties have come under scrutiny only in the recent years [4–6]. Quite interestingly, the damage tolerance of these nanotwinned materials is found to be demonstrably improved compared to the more conventional counterparts. In this context, we note the importance of further studies, specifically addressing the microstructure-sensitive crack growth regime. In particular, it would be of great interest to establish the relevant factors governing the near-threshold crack advance mechanism(s) in the presence of nano-scale twins. Essentially, the very nature of the problem necessitates a synergistic approach between sophisticated experimental characterizations and the requisite theoretical underpinnings at the microscopic level. Recently, there have been considerable developments in connecting atomic scale physical process to the macroscale deformation behaviors [7–9]. To that end, we first probe into the experimental crack propagation behavior(s) of nanotwinned Ni–2.89 wt.% Co alloy, and then rationalize the findings with a physical theory. Our modeling strategy is twofold involving both non-continuum and continuum analyses: (1) studying the role of coherent twin boundaries on the crack-emitted slip (via atomic-scale simulations), and (2) examining the cyclic crack advancement metrics influenced by nano-sized twins (via continuum scale simulations).

1.2. Experimental damage properties

As the crack tip is a source of dislocations [10] and dislocation patterns evolving under cyclic loading are directly related to the twin thickness [11], it is reasonable to expect that twin volume fraction will affect the fatigue damage impedance of nanotwinned metals/alloys. Singh et al. [12] reported that decreased inter-twin spacing results in a substantial improvement of fatigue crack growth resistance in nanotwinned Cu. Similar enhancement in the damage properties was also noted by Sangid et al. [13] for the case of electrodeposited nanotwinned Ni–Co alloys. In

* Corresponding author. Tel.: +1 217 333 4112; fax: +1 217 244 6534.
E-mail address: huseyin@illinois.edu (H. Sehitoglu).

http://dx.doi.org/10.1016/j.ijfatigue.2015.11.012
0142-1123/

Nomenclature

FCG, CTB	fatigue crack growth, coherent twin boundary
MD, GSFE	molecular dynamics, generalized stacking fault energy
HT	heat treated
EAM	embedded atom method
DIC	Digital Image Correlation
da/dN	FCG rate
a	crack length
N	number of cycles
b_r	magnitude of residual Burgers vector
K, K_{max}, K_{open}	stress intensity factor (SIF), maximum SIF, opening SIF
$\Delta K, \Delta K_{th}, \Delta K_{eff}^{th}$	SIF range, threshold SIF range, effective threshold SIF range
k_{IIIa}, k_{IIIe}	local applied SIF, critical SIF to emit slip
R	load ratio
G	shear modulus
E^{misfit}, $E^{elastic}$	misfit and elastic energy
v	Poisson's ratio
d	lattice constant
t, s	twin thickness, twin spacing respectively
θ	angle between crack and slip paths
r	radial distance measured from the crack tip
p	Paris law exponent
C	Paris law proportionality constant
T	T stress
Tw	twin coordinate frame
n^C	number of crystal dislocations, number of pre-existent dislocations
n^{emit}	number of dislocations emitted from the crack tip
n^{res}	number of residual dislocations
Δu	irreversible crack tip displacement in Burger vector's direction
ε^{max}	maximum strain at the crack tip plastic zone
ε^{irr}	irreversible strain at the crack tip
x, y	horizontal and vertical positions of dislocations respectively
$\sigma_F, \sigma_F^{Barrier}$	unobstructed and obstructed slip glide stress

particular, the electron microscopy of fatigued Ni–Co alloys indicated a widespread presence of slip-mediated plasticity subjected to the twins. The foregoing literature findings strongly suggest that the mechanistic origin of the observed near-threshold damage properties can be attributed to the outcome of massive slip–twin interactions. Particularly, we note that the cyclic crack increment would be directly proportional to the degree of crack-emitted slip irreversibility, which would be governed by a specific outcome of the slip–twin interaction [14–16]. In other words, the greatest resistance to the cyclic crack growth would intuitively originate from the case of slip–twin interception with the least extent of slip irreversibility. Hence, it is imperative to pinpoint such slip interception mechanism to better understand the mechanistic origin of the reportedly superior damage impedance of nanotwinned materials.

1.3. Theoretical developments

Considerable progress has been made in understanding the role of CTBs on transferring dislocation slip [17,18]. Early literature noted that a CTB can allow: (1) full transmission of slip with no residual slip on the interface (i.e. the cross-slip through the boundary), (2) partial transmission when an interfacial residual slip develops and (3) no transmission whatsoever (i.e. the incorporation onto the boundary) [19]. These interaction outcomes are strongly dependent on the local stress state and the geometry of the approaching slip [20]. The effects of these reaction outcomes on the fatigue crack propagation properties have most recently been addressed by Chowdhury et al. [16,21,22]. Particularly, they considered the case of non-zero residual dislocation, and demonstrated how the irreversibility of the associated slip trajectory would be influenced.

Earlier, Pippan et al. [23,24] devised a continuum dislocation model to demonstrate the importance of considering irreversibility of discrete slip (in the presence/absence of obstacles) to quantify fatigue threshold metrics. A complete analysis of the cyclic slip–barrier interaction outcomes i.e. the role of residual slip, from a non-continuum standpoint could provide useful mechanistic insight in this regard. It can be inferred from the Chowdhury et al.'s study [16,21,22] that a lower magnitude of residual slip promotes the overall slip reversibility, and hence decelerates the attendant crack growth rate.

Given the foregoing background, the cross-slip of a screw dislocation is particularly noteworthy, and bears important mechanistic implications regarding the fatigue crack growth resistance. The cross-slip at a twin boundary would occur with the least amount of frictional resistance due to the absence of residual slip [19]. Most notably, under cyclic loading, the lattice impedances for forward and reverse cross-slip would essentially be similar, unlike other reaction types (where reverse glide would be more difficult due to the residual dislocation) [16]. In other words, the cross-slip can be associated with the least irreversible dislocation trajectory during fatigue loading.

1.4. Current approach

In light of the foregoing discussion, one can identify the governing factors for the near-threshold crack growth properties of nanotwinned materials, namely, the characteristic twin dimensions (i.e. thickness and spacing), the initial dislocation density and slip–twin interaction types. This paper aims to analyze the effects of these factors in cross-slip configuration. First, fatigue crack growth experiments are performed on electrodeposited nanotwinned Ni–2.89 wt.% Co before and after heat treatment. We characterize the threshold stress intensity factor range and the ensuing Paris regime of nanotwinned Ni–Co for both cases. Then, we employ a high magnification, *in situ* DIC technique to quantify the degree of axial, cyclic irreversible strain at the crack tip. Transmission electron microscopy (TEM) is utilized to note the microstructural differences between the pre- and post-heat treated materials. On theoretical grounds, we conduct molecular dynamics (MD) simulations to investigate the cross-slip of a crack-emitted dislocation across a CTB. Particularly, the energy barrier for cross-slip is quantified and then used in a Peierls–Nabarro formalism [25,26] to extract the associated lattice friction stress. Thus-computed friction stresses are used as an important ingredient in a continuum scale dislocation motion simulation. These fatigue crack growth simulations, informed by the atomistically calculated glide strengths are then used to isolate the role of twin boundaries on the damage metrics of the Ni–Co alloys. In essence, we propose a generic modeling platform to test the role of friction stress, twin dimension and pre-existent dislocation density (in the near-tip area) on the damage resistances in terms of the effective threshold stress intensity range. In doing so, no

empiricism is invoked. The theoretical results serve to provide a physical rationale for the observed experimental fatigue behaviors.

2. Methods

2.1. Experiments

The as-received Ni–2.89 wt.% Co, supplied by NiCoForm Incorporation [27], was heat treated for 4 h at 600 °C (the post-treatment material being designated as Ni–Co 600 HT henceforth). This promotes a microstructure with coarser grains and twins as well as minimizing the dislocation density. The average grain size for pre-treatment Ni–Co was measured as 97 nm while for Ni–Co 600 HT as 430 nm using the linear intercept method on the TEM images. Further details about the materials preparation and the fatigue crack growth tests could be found in [13].

To measure near-tip strains in the current work, the stress controlled fatigue experiments under the same aforementioned conditions, with the applied stress range of 13.75–275 MPa, were conducted on both Ni–Co and Ni–Co 600 HT by using SEM Tester load frame under Olympus BX51M optical microscope. SEM Tester allows running in-situ experiments under optical microscope and Scanning Electron Microscope (SEM) so that high magnification images for DIC can be collected *in situ*. The resolution of the images at this high magnification experiment is 0.21 μm/pix. An illustration of the general methodology for correlating ε^{max}, and v fields near the crack tip can be seen in Fig. 1.

Multiple experiments were conducted to examine the scatteredness in the trends, which was found very negligible.

2.2. Molecular dynamics

MD simulations were conducted by LAMMPS software [28] using a Ni–Co embedded-atom interatomic potential (Ni–2.78 wt. % Co composition) based on an EAM pair-potential from the literature [29]. In order to simulate the cross-slip at a twin boundary, an annealing twin was constructed. More details regarding the MD procedure adopted for the current work could be found at [30]. The snapshots from the MD simulation were analyzed by VMD [31] and Atom Eye [32] visualization tools.

3. Results

3.1. Fatigue crack growth experiments

In the fatigue crack growth experiments, the plane stress vertical displacement field, v, at the crack tip was captured for the each cycle, and regressed using Eq. (1), to fit the stress intensity factor, K_I (following the same procedure as outlined in [13]).

$$v = \frac{K_I}{G}\sqrt{\frac{r}{2\pi}}\sin\left(\frac{\theta}{2}\right)\left[\frac{1}{2}\left(\frac{3-v}{1+v}+1\right)-\cos\left(\frac{\theta}{2}\right)\right] - \frac{1}{2G}\left(\frac{v}{1+v}\right)Tr\sin(\theta)+Ar\ \cos(\theta)+B \quad (1)$$

where r is the radial distance measured from the crack tip, G the shear modulus (50 GPa), v the Poisson's ratio and θ is the angle to horizontal axis. The A and B terms correspond to the rigid body rotation and the translation respectively. The parameter T represents the uniform stress component in the horizontal direction (which is also commonly known as T-stress).

The effective stress intensity factor range, ΔK_{eff}, which is responsible for the crack propagation is obtained from Eq. (2). An accurate measurement of the K_{open} level is extracted from the digital image correlation analyses.

$$\Delta K_{eff} = K_{max} - K_{open} \quad (2)$$

The crack growth rates measured for Ni–Co and Ni–Co 600 HT were fitted into the Paris Law [33] in Eq. (3) to study the relevant coefficients.

$$\frac{da}{dN} = C(K_{max}-K_{open})^p = C(\Delta K_{eff})^p \quad (3)$$

The measured fatigue crack growth rate versus ΔK_{eff} data are presented in Fig. 2. The slope of the Paris regime, p, was measured to be 1.3 and 2.0 for Ni–Co and Ni–Co 600 HT respectively. Typically, the value of p ranges from 2 to 7 [34] for conventional coarse-grain ductile metals. Therefore, the current materials demonstrably possess superior fatigue crack growth resistance. The measured Paris Law coefficients and the effective threshold stress intensity factor range, ΔK_{eff}^{th}, are summarized in Table 1.

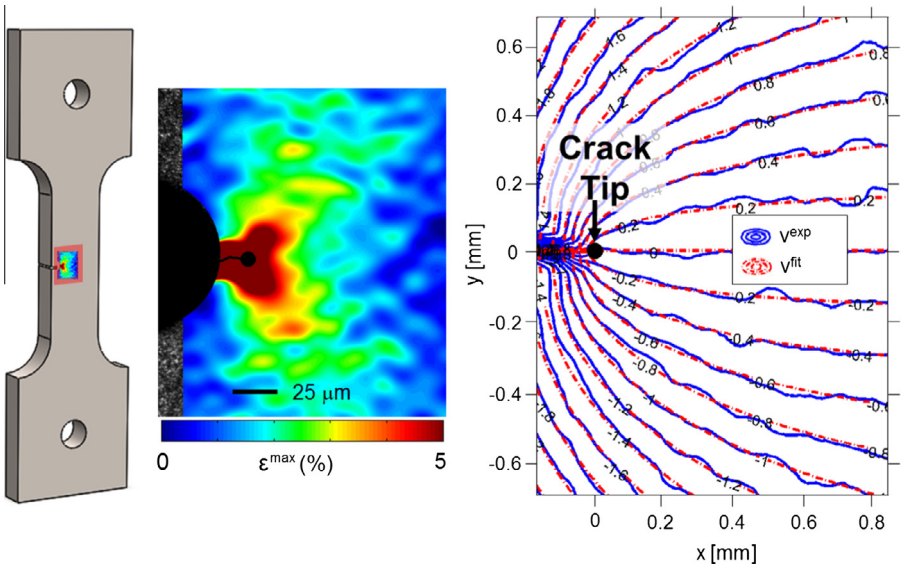

Fig. 1. The schematic on the left shows the notched fatigue test specimen. The figure in the middle presents the strain field correlation for ε^{max} using DIC. The rightmost figure is a contour plot for vertical displacement field correlation.

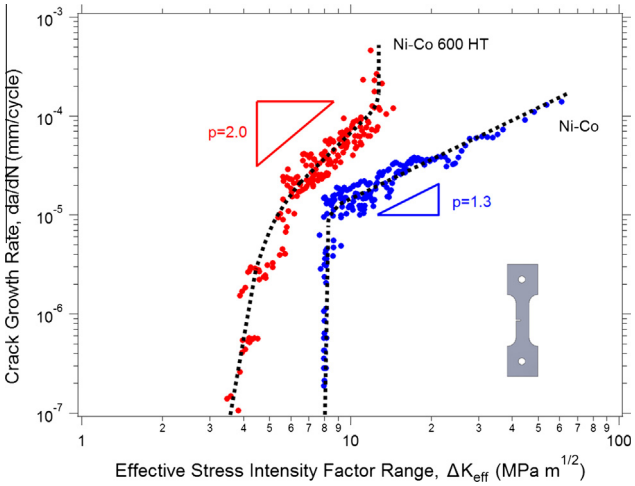

Fig. 2. Fatigue crack growth rates for Ni–Co and Ni–Co 600 HT plotted versus effective stress intensity factor range.

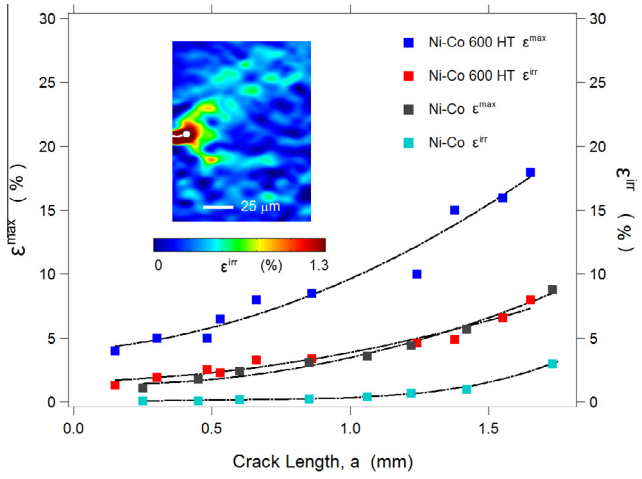

Fig. 3. The correlation of the parameters ε^{max} and ε^{irr} with crack length, a. The inset DIC image shows ε^{max} field correlation at a crack length of 150 μm. Ni–Co 600 HT exhibits higher slip irreversibility near the crack tip compared to Ni–Co.

Table 1
Paris law coefficients and the effective threshold stress intensity factor ranges of Ni–Co and Ni–Co 600 HT.

Specimen	p	C	ΔK_{eff}^{th}
Ni–Co	1.3	9.0×10^{-7}	8.0 MPa$\sqrt{m}$
Ni–Co 600 HT	2.0	5.0×10^{-7}	3.5 MPa$\sqrt{m}$

3.2. High magnification fatigue crack growth experiments

The maximum and the irreversible plastic strain at the cracktip (ε^{max} and ε^{irr} respectively) are measured at different crack lengths as in Fig. 3. Both ε^{max} and ε^{irr} in Ni–Co 600 HT are observed to be larger than Ni–Co. The higher magnitude of ε^{irr} in Ni–Co 600 HT is believed to be reason for the lower ΔK_{eff}^{th} thereof. Note that both of ε^{max} and ε^{irr} increases with the crack length. The DIC image placed as an inset of Fig. 3 shows the ε^{irr} field accumulated near the crack tip in Ni–Co 600 HT for a crack length of 150 μm.

3.3. Microstructure study using transmission electron microscopy (TEM)

TEM images are taken both from the undeformed and the fatigued specimens. In Fig. 4a, the microstructure of the undeformed Ni–Co is characterized by nanograins and nanotwins. Additionally, the presence of dislocations in the undeformed Ni–Co sample can be seen in Fig. 4a. The arrow points to the dislocations bowing out from the twin and grain boundaries. The dislocations are observed to be clustered near the twin and grain boundaries after the fatigue deformation in Fig. 4b.

Following the heat treatment, the undeformed material undergoes grain and twin coarsening as can be seen in Fig. 5a. The dislocation density is observed to be lowered, compared to Ni–Co in undeformed sample. The "t" letter indicates the twin thickness, later to be used in modeling. As a result of cyclic deformation, in Fig. 5b, the dislocation density increases. Twin and grain boundaries are observed to be the preferred sites for slip localizations.

To model the experimental observations, we conduct atomistic and continuum scale simulations described as follows.

4. Modeling

4.1. Molecular dynamics simulations

4.1.1. Study of slip–twin interaction mechanism

MD simulations were conducted in order to study the nature of crack-emitted slip interacting with a coherent twin boundary (CTB). A single crystal of Ni–2.78% Co is constructed with an annealing twin of a finite thickness [16]. A dislocation source placed in the vicinity of one of the coherent twin boundaries (CTB). With applied loads, an extended screw dislocation (consisting of a leading and a trailing partial) approaches the CTB from the source on the most favorable slip plane. On intercepting the CTB, it is transmitted inside the twin in the form of a new pair of a leading and a trailing partial. There is no residual dislocation present on the twin boundary at the end of this reaction (Fig. 6). This interaction is essentially a cross-slip phenomenon. The same reactions occur on reversing the loading. The forward and reverse reactions were summarized in Eqs. (4) and (5) respectively. The "Tw" subscript denotes twin coordinate.

$$\frac{d}{6}[\bar{2}1\bar{1}] + \frac{d}{6}[\bar{1}21] \rightarrow \frac{d}{2}[\bar{1}10] \tag{4}$$

$$\frac{d}{2}[\bar{1}10] \rightarrow \frac{d}{6}[1\bar{2}\bar{1}]_{Tw} + \frac{d}{6}[2\bar{1}1]_{Tw} \tag{5}$$

Next, the frictional stress for the cross-slip at the CTB is calculated using Peierls–Nabarro (PN) formulations [35]. The most important input to the PN model is the unstable stacking fault energy, γ_{us}, the extrinsic value of which is calculated (discussed in more details in Section 4.3). Using the frictional stress, based on the MD simulations, a continuum dislocation based fatigue simulation model is proposed.

4.2. Continuum dislocation motion simulations

Now, we propose a continuum based fatigue model, which also uses input from the MD calculations. A mode III crack, emitting screw dislocations, is placed near an annealing twin, and the resulting irreversible motion of dislocations are quantified under a single load cycle with a load ratio, $R = 0.05$. The applied stress intensity factor, K_{IIIa}, is cycled between K_{min} to K_{max} incrementally. Unless otherwise stated, the crystal configuration is modeled as dislocation free. The general geometry and loading used for K_{IIIa} increments throughout the dislocation motion simulations are illustrated in Fig. 7.

The dislocation emission from the crack is controlled by the local stress intensity factor at the crack tip, k_{III}, which is the same as K_{IIIa} in the absence of dislocations. When k_{III} reaches the critical local stress intensity factor value for dislocation emission, k_{IIIe}, a positive screw dislocation is emitted from the crack tip and its

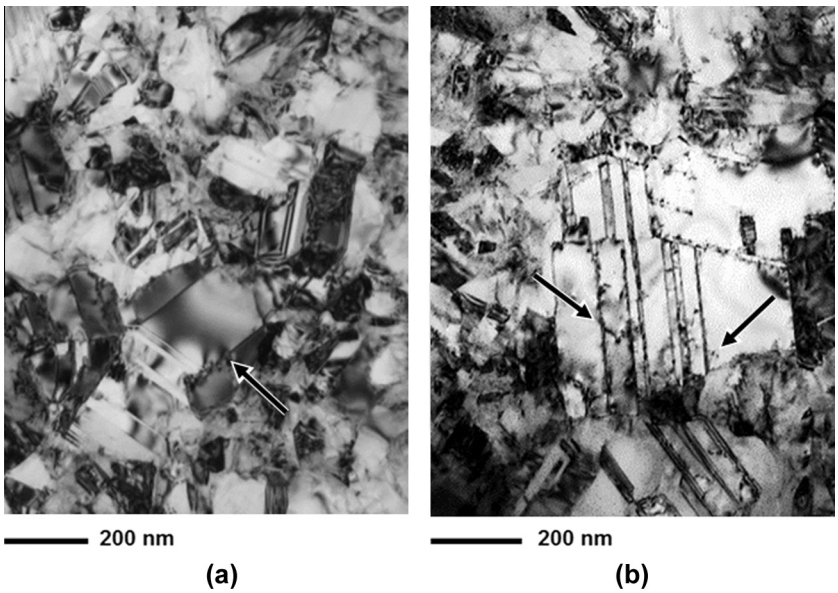

Fig. 4. (a) The undeformed microstructure of Ni–Co. The nanotwins with pre-existent dislocation are visible. (b) Dislocation–twin interactions resulting from cyclic loading can be seen.

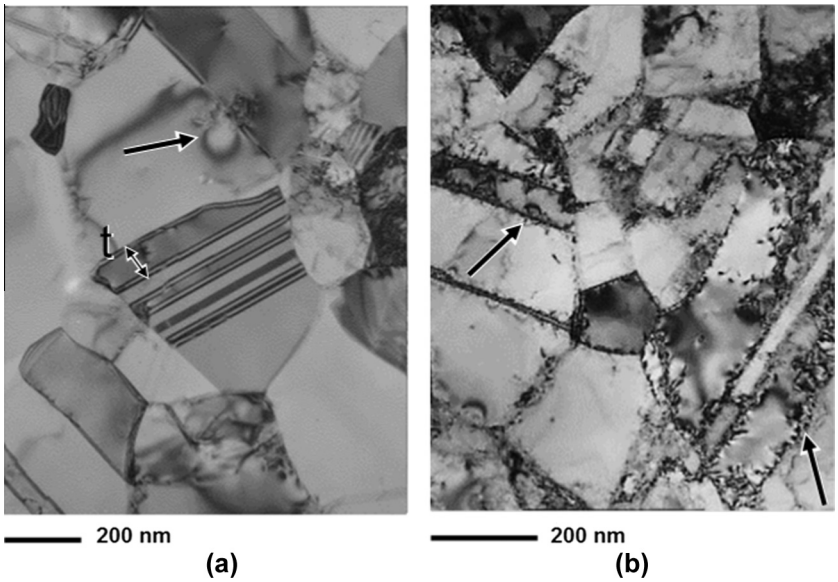

Fig. 5. (a) Ni–Co 600 HT microstructure before deformation. The twins and the grains are coarsened. Lower dislocation density compared to Ni–Co is observed as a result of the recovery processes. The '*t*' indicates twin thickness. (b) Ni–Co 600 HT microstructure after a fatigue experiment.

equilibrium position is evaluated by invoking force equilibrium. k_{IIIe} value for the dislocation emission is provided in Eq. (6) where x_c is the core width of the emitted dislocation, which is 4.2 Angstrom for Ni–2.89 wt.% Co [36].

$$k_{\mathrm{IIIe}} = \frac{Gb_i}{\sqrt{8\pi x_c}} + \sqrt{2\pi x_c}\sigma_F \tag{6}$$

The force acting on the *i*th dislocation in the matrix is evaluated according to Eq. (7) where $\eta = \sqrt{-1}, r_i = \sqrt{x_i^2 + y_i^2}$ and $\theta_i = a\tan(y_i/x_i)$ [37]. b_i is the Burgers' vector of the corresponding dislocation where $b = |1/2[\bar{1}\,1\,0]|$. Eq. (7) was solved for x_i values to determine dislocation positions at each increment of K_{IIIa}. The y_i values can be written as a function of x_i's by using the simple trigonometric relations for the configurations described in Figs. 6 and 7. For the negative dislocations, the sign of the Burgers' vector is changed from positive to negative.

$$\frac{K_{IIIa}b_i}{\sqrt{2\pi r_i}}\cos\left(\frac{\theta_i}{2}\right) + \sum_{\substack{i=1\\ i\neq j}}^{n}\mathrm{Re}\left(\frac{Gb_j}{4\pi\sqrt{x_i+\eta y_i}}\Phi\right)b_i - \lambda\frac{Gb_i}{4\pi r_i}\cos^2\left(\frac{\theta_i}{2}\right)b_i - \sigma_F b_i = 0 \tag{7}$$

where Φ is given as in Eq. (8).

$$\Phi = \frac{1}{\sqrt{x_i+\eta y_i} - \sqrt{x_j+\eta y_j}} - \frac{1}{\sqrt{x_i+\eta y_i} + \sqrt{x_j-\eta y_j}} \tag{8}$$

In the equations above n is the total number of dislocations (which could be either the number of dislocations emitted from the crack tip i.e. $n = n^{\mathrm{emit}}$ or the initially present crystal dislocations i.e. $n = n^{C}$). The parameter λ is assumed to be unity, and σ_F is the unobstructed friction stress for pure Ni–Co which is predicted to be 60 MPa (as detailed in the following section). σ_F would be replaced with $\sigma_F^{\mathrm{Barrier}}$ (145 MPa) if the crack-emitted dislocation is very close to the twin boundaries (within 5*b*). This proximity

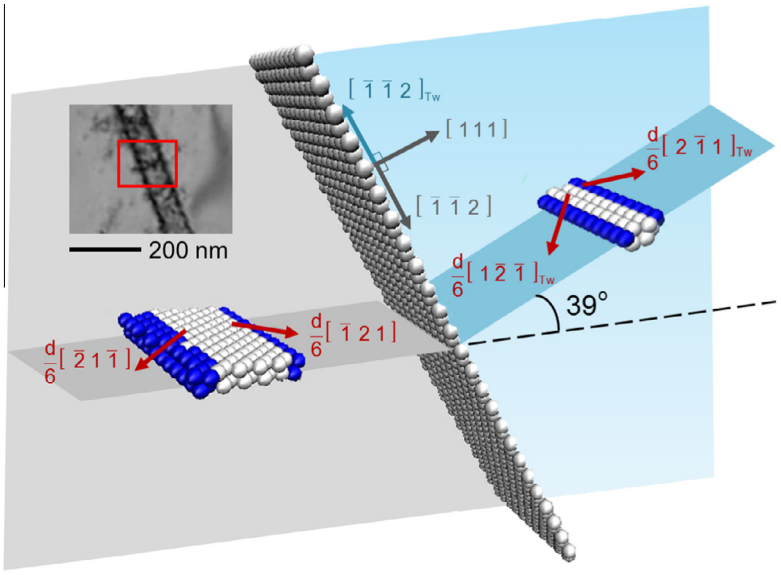

Fig. 6. The dissociated screw dislocation approaches to the coherent twin boundary and cross-slips. There is 39° angle difference between incoming and outgoing slip planes. The inset is a TEM image of the Ni–Co 600 HT fatigued specimen demonstrating dislocations around a twin boundary, a situation which is simulated for the cross-slip case.

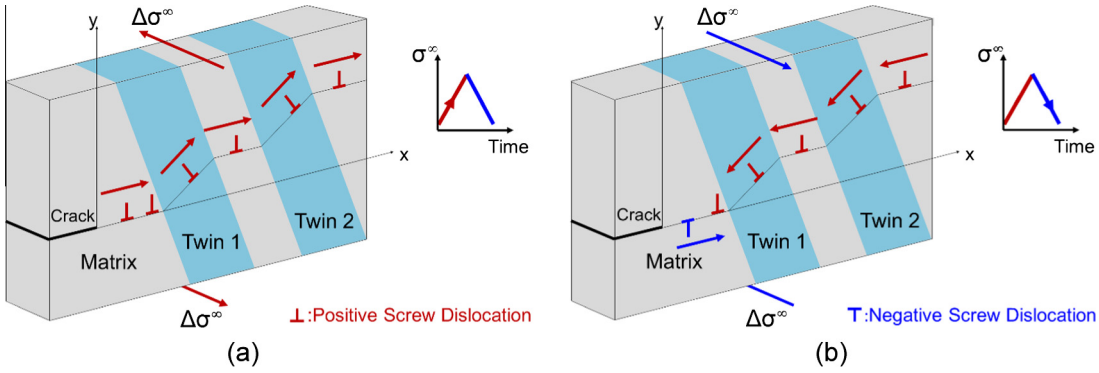

Fig. 7. (a) The loading configuration of the dislocation based fatigue model under mode III. The emitted positive screw dislocations cross-slip a twin boundary. Inside the twin lamellae, the dislocation glide planes make an angle of 39° with the planes in the matrix, which results in a decrease of resolved shear stress on the glide plane. (b) The unloading configuration where the twin boundaries affect the glide path irreversibility.

condition is determined from the Generalized Stacking Fault Energy (GSFE) curve [38] calculated from the MD simulations. The GSFE curve resulting from the slip transmission across a CTB differs from the one in a perfect crystalline within ±5b distance of a CTB. The first term in Eq. (7) represents the force field due to the applied stress intensity factor whereas the second term represents the interaction of the dislocations among each other. The third term accounts for the image force of the crack surfaces.

The governing equation for the twin lamellae are given in Eq. (9) [36,39]. Note that Eqs. (7) and (9) ought to be solved simultaneously.

$$\frac{K_{IIIa}b_i}{\sqrt{2\pi r_i}}\cos\left(39^\circ-\frac{\theta_i}{2}\right)+\frac{Gb_i^2(\sin(39^\circ-\theta_i)-\sin(39^o))}{4\pi r_i\sin(\theta_i)} + \sum_{\substack{j=1\\ i\neq j}}^{n}\mathrm{Re}\left(\frac{Gb_j}{4\pi\sqrt{x_i+\eta y_i}}\Phi\right)\cos(39^\circ) - \sum_{\substack{j=1\\ i\neq j}}^{n}\mathrm{Im}\left(\frac{Gb_j}{4\pi\sqrt{x_i+\eta y_i}}\Phi\right)\sin(39^\circ)-\sigma_F b_i=0 \tag{9}$$

In the presence of near-tip dislocations, the local stress intensity factor at the crack tip, k_{III} is not equal to K_{IIIa}, anymore. The positive screw dislocations cause shielding at the crack tip during loading and hence lower k_{III}. Eq. (10) shows the evaluation of k_{III} in presence of dislocations ahead of the crack tip.

$$k_{III}=K_{IIIa}-\sum_{i=1}^{n}\frac{Gb_i}{\sqrt{2\pi r_i}}\cos\left(\frac{\theta_i}{2}\right) \tag{10}$$

During unloading, there is no dislocation motion unless the applied forces acting on the dislocations are lower than $-\sigma_F b_i$ or $-\sigma_F^{\mathrm{Barrier}}b_i$ (i.e. at the CTB) depending on their locations. At this critical value, the positive screw dislocations begin to move back to the crack tip. As the dislocations get closer to the crack tip, the local stress intensity factor decreases and at some point becomes lower than $-k_{IIIe}$ which is the critical value for negative screw dislocation emission. A negative dislocation cause increase in k_{III} at the crack tip unlike a positive one. The interaction of positive and negative dislocations may result in residual dislocations left at the end of the cycle that is quantified as n^{res}. The cyclic irreversible crack tip displacement in Burgers' vector direction, Δu, is quantified in Eq. (11), below.

$$\Delta u=n^{\mathrm{res}}b \tag{11}$$

Theoretically, the smallest Δu value can be chosen as b, which corresponds to one dislocation.

4.3. Peierls–Nabarro formulation

The lattice frictional stresses for both free glide (σ_F) and the glide across a CTB ($\sigma_F^{\text{Barrier}}$) were evaluated using Peierls–Nabarro formulations [40–43]. Eq. (12) describes the determination of $\sigma_F^{\text{Barrier}}$ where u^* is the dislocation translation distance [41].

$$\sigma_F^{\text{Barrier}} = \max\left(\frac{1}{b}\frac{dE^{\text{total}}}{du^*}\right) \tag{12}$$

The total energy requirement is evaluated by summing up misfit energy, E^{misfit}, elastic energy, E^{elastic}, and subtracting the external work done, W for a single full dislocation per unit length as in Eq. (13).

$$E^{\text{total}} = E^{\text{misfit}} + E^{\text{elastic}} - W \tag{13}$$

The details about individual energy terms were provided in Appendix A for the interested reader.

For cross-glide of a full screw dislocation across CTB, $\sigma_F^{\text{Barrier}}$ value is 145 MPa while the free glide resistance σ_F is found to be 60 MPa. The configuration corresponding to cross-slip exerts the lowest resistance against dislocation transmission owing to the absence of any b_r. Quantification of $\sigma_F^{\text{Barrier}}$ according to the varying magnitude of b_r is shown in Fig. 8 [35].

4.4. Simulated microstructure effects on fatigue threshold

Different scenarios were devised in order to quantify the trends in the fatigue threshold values of Ni–Co. The cyclic irreversibility values, Δu, for the threshold condition were chosen as $10b$ (i.e. 2.5 nm).

The friction stress at the twin boundary was set equal to 145 MPa (i.e. for cross-slip), 250 MPa and finally 60 MPa which is same as the unobstructed glide friction stress, σ_F. For 60 MPa case, due to the change in the orientation of slip systems across a CTB, the applied shear stress on a dislocation is reduced inside the twin lamellae. In Fig. 9, the resulting $\Delta K_{\text{eff}}^{\text{th}}$ values for the three cases with varying twin thickness (chosen equal to inter-twin spacing for this case) values are presented. The simulation results indicate that $\Delta K_{\text{eff}}^{\text{th}}$ increases as the barrier strength is elevated. For example, for 10 nm thick twin lamellae, $\Delta K_{\text{eff}}^{\text{th}}$ calculated to be shifting from

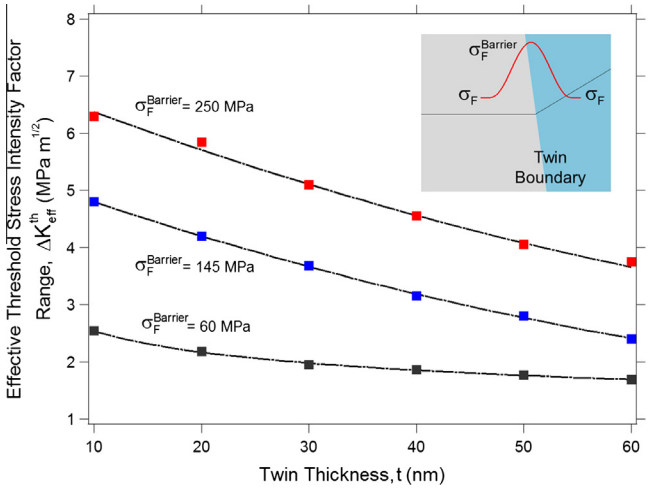

Fig. 9. The barrier friction stress (i.e. the strength of the CTB to slip incidence) has a significant effect on the crack growth threshold. As the strength of the CTB increases, so does the effective threshold stress intensity factor range.

2.54 MPa $\sqrt{m}$ to 4.8 MPa $\sqrt{m}$ and 6.3 MPa $\sqrt{m}$, as $\sigma_F^{\text{Barrier}}$, increases from 60 MPa to 145 MPa and 250 MPa respectively. The same trend is also valid for the other twin thickness values in the simulated range of 10–60 nm, although the most prominent difference was evaluated for 10 nm case.

The high magnification experiments revealed that ε^{irr} accumulates at the crack tip at higher rates as the crack advances. In the dislocation motion simulations, a similar effect has been observed for Δu values which are plotted with respect to the corresponding crack lengths in Fig. 10. The number of crack-emitted dislocations, n^{emit}, were also added in this plot. Because it reflects the crack tip shielding and the irreversible cyclic crack tip displacement, Δu, correlation. Fig. 10 demonstrates both n^{emit} and Δu show similar trends to ε^{max} and ε^{irr} measured in the experiments.

In order to quantify the effects of pre-existent near-tip dislocations, we placed 2 and 3 crystal dislocations in the matrix region between the crack tip and the first twin lamella. The inter-twin spacing and twin thickness are taken as equal. The resulting threshold values for this scenario are shown in Fig. 11. Due to shielding effects, the number of dislocations emitted from the

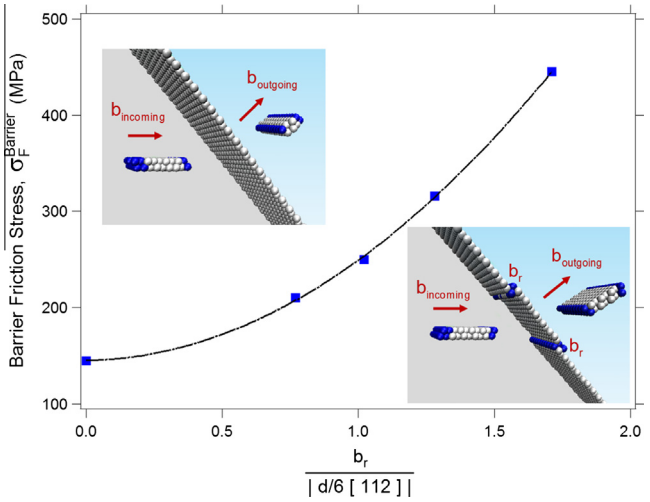

Fig. 8. The relation between the magnitude of residual Burgers vector and the magnitude of the barrier friction stress. As b_r increases in magnitude, the friction stress amplification gets more pronounced. The minimum amplification is evaluated for cross-slip configuration as seen at $b_r = 0$.

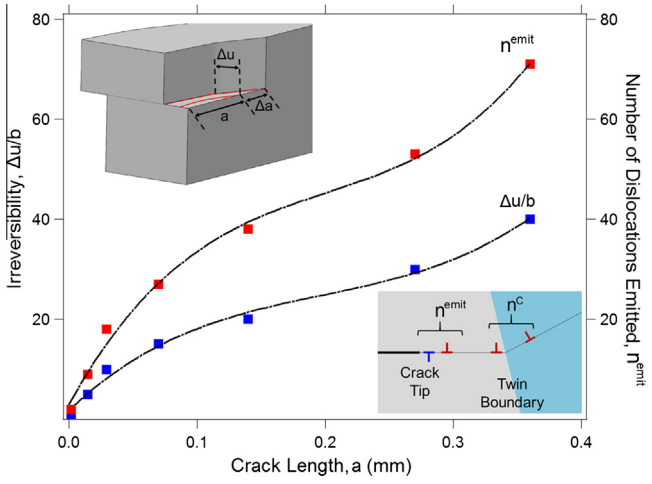

Fig. 10. Quantification of the degree of irreversibility at the crack-tip as the crack length continues to grow in the dislocation based simulations. The trend complies with the experimental measurements as presented earlier.

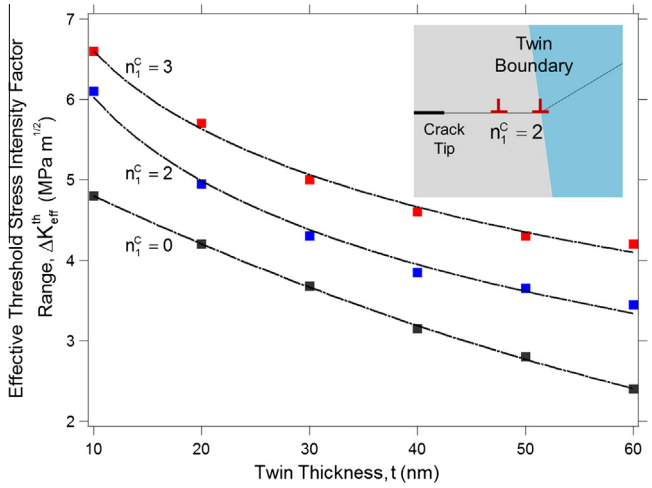

Fig. 11. The effect of the number of pre-existent dislocations, n^C (between the crack-tip and the twin boundary) used in the dislocation based simulations. It clearly has a significant effect on ΔK_{eff}^{th}.

crack tip decreases and the total irreversibility is reduced. The simulation results show a significant increase in ΔK_{eff}^{th} for the case of pre-existent slip compared to the initially dislocation free scenarios. Although ΔK_{eff}^{th} is 4.8 MPa$\sqrt{m}$ for the dislocation free scenario ($n^C = 0$) for 10 nm twin thickness; in the presence of and 2 and 3 crystal dislocations, e.g. $n^C = 2$ and $n^C = 3$ respectively, ΔK_{eff}^{th} increases to 6.1 MPa$\sqrt{m}$ and 6.6 MPa$\sqrt{m}$.

Two scenarios, keeping constant t and s at 30 nm and varying the other, were devised in order to quantify the individual effects of these two geometrical parameters. The results shown in Fig. 12 indicate that decrease in either t or s levels results in an increased ΔK_{eff}^{th}. ΔK_{eff}^{th} is elevated to 4.4 from 2.7 MPa$\sqrt{m}$ in case of decreasing t from 60 nm to 10 nm. The same amount of refinement of inter-twin spacing results in an increase of ΔK_{eff}^{th} from 2.9 to 4.8 MPa $\sqrt{m}$. These results comply with experimental results for Ni–Co and Ni–Co 600 HT since Ni–Co has higher volume fraction of twins which results in lower s and t.

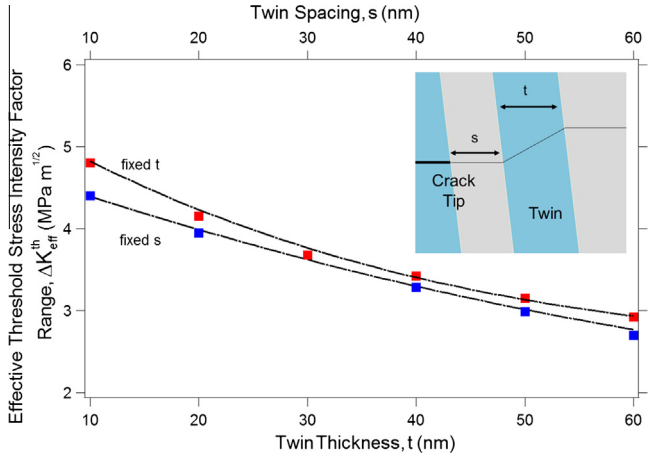

Fig. 12. The decreases in the twin thickness, t, as well as spacing, s, improve the fatigue damage impedance by elevating threshold value. The blue data represent variation of t (at a fixed s value of 30 nm). On the other hand, the red data represent the change in threshold value under fixed t of 30 nm. (For interpretation of the references to colour in this figure legend, the reader is referred to the web version of this article.)

4.5. Comparison between simulated and experimental results

In order to compare the Mode III simulation results with the experimental data corresponding to Ni–Co and Ni–Co 600 HT in Mode I, Δu values evaluated in the simulations must be converted to the equivalent Mode I da/dN. In Mode III, the screw dislocations are emitted along the slip planes parallel to the crack plane. However, under Mode I loading, the critical local stress intensity factor for dislocation emission is evaluated to be minimized at an inclination angle of 70.5° [37]. Hence, the dislocations are emitted along the slip plane at an inclination of 70.5° in Mode I. In that regard using Eq. (14) enables to project the Mode III irreversibility values (in the simulations) onto the experimental data measured in Mode I. In Eq. (14), a trigonometric factor of cos(70.5°) is included to convert Δu values to Δa values in Mode I [44].

$$\frac{da}{dN} = \Delta u \cos(70.5^\circ) = n^{res} b \cos(70.5^\circ) \tag{14}$$

Next, we attempt to predict the multiple threshold behaviors as observed experimentally. As elucidated earlier, depending on the twin thickness/spacing and/or pre-existent dislocation density, the ΔK_{eff}^{th} levels would vary substantially. We predict the experimental levels of the threshold by tailoring these factors as presented in Fig. 13. The simulations demonstrated that different bands of predictions (represented by red, blue and green) corresponding to the average twin thickness values (and also twin spacing, s) of 55 nm, 40 nm and 25 nm respectively. The bands were bounded with a variation of ±5 nm. The yellow band is obtained by considering the twin thickness and spacing values varying between 55 and 40 nm. The red, blue and green bands correspond to 2, 3 and 4 crystal dislocations per each twin and matrix lamella. These results in Fig. 13 indicate that variations in these aforementioned parameters can actually capture different ΔK_{eff} values from the experiments.

Agreement of the predictions with the theory in Fig. 13 bears important mechanistic implications regarding the NiCo threshold behaviors. As observed from the TEM analyses, the twin thickness/spacing and the dislocation density differ significantly. Therefore, given the simulation-observed sensitivity of the near-threshold fatigue behavior on the foregoing factors, it is only reasonable to assume that the experimentally measured scatter in the threshold regimes is a result of various magnitudes of twin thickness/spacing and dislocation density.

5. Discussion

From the experimental results (Fig. 2), we note that the heat-treated Ni–Co has lower fatigue crack growth impedance compared to as-received materials both in near threshold regime and Stage II. The DIC-measured values for near-tip irreversible strain ε^{irr} suggest that the slip irreversibility is higher for Ni–Co 600 HT compared to the as-received Ni–Co. With the experimental measurement of effective stress intensity from the displacement fields, the operational extrinsic effects (e.g. closure phenomena) are already accounted. From the TEM analyses, the principal difference between the heat-treated and non-heat-treated materials is observed in the distribution of relative twin thickness and spacing. The heat-treated materials underwent coarsening in terms of these characteristic twin dimensions. Hence, the observed difference in ΔK_{eff}^{th} values can be reasonably attributed to the intrinsic effects (e.g. twin thickness/spacing), which dictates the crack growth behavior.

The current experimental results clearly demonstrate that nanotwinned Ni–Co alloys possess superior fatigue resistances (as indicated by the currently measured ΔK_{eff}^{th} levels) with refinement

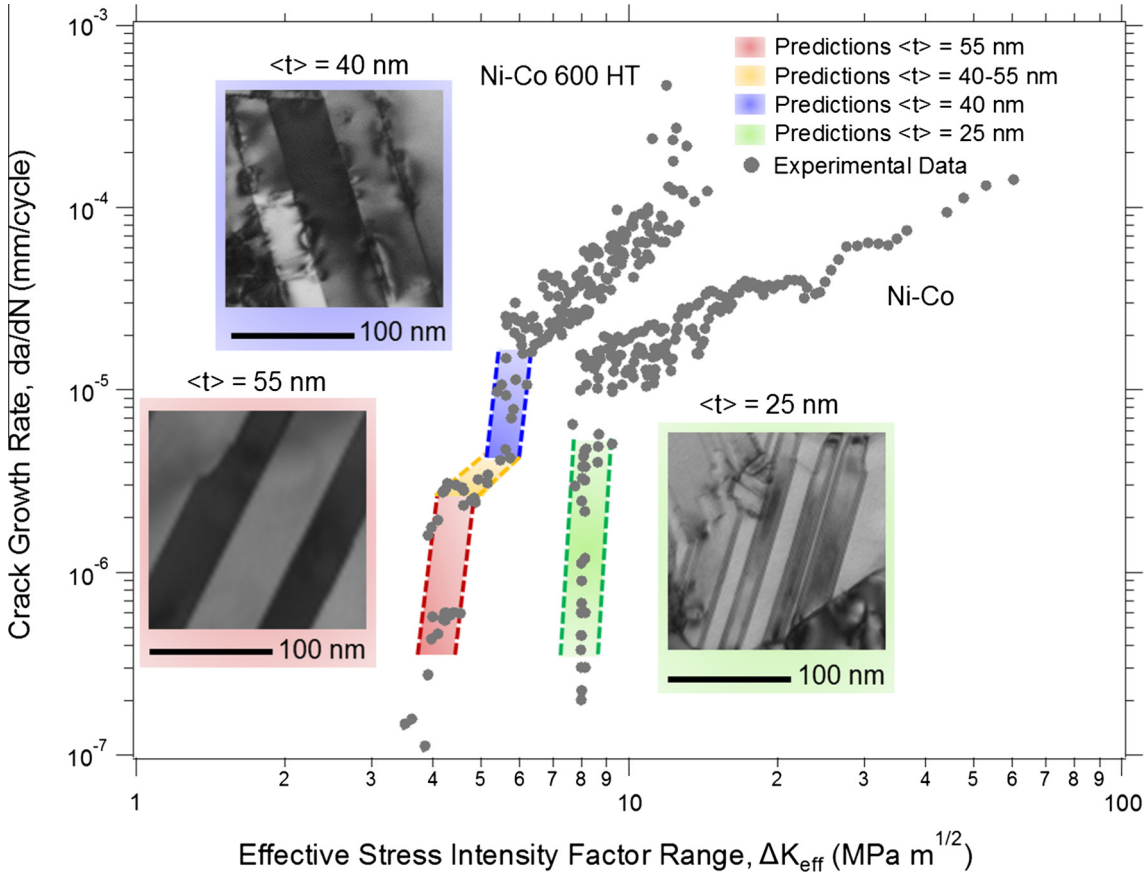

Fig. 13. Superimposition of experimental and theoretical da/dN vs ΔK_{eff} for Ni–Co and Ni–Co 600 HT. The predicted values are presented as colored bands to provide bounds for the experimental values. The variations in the predictions are obtained based on a range of averaged values for twin thickness, spacing and crystal dislocation density from the TEM images. The averaged $\langle s \rangle$ values are of the same values as that of $\langle t \rangle$, and the number of dislocations, n^C are 2, 3 and 4 for red, blue and green respectively. (For interpretation of the references to colour in this figure legend, the reader is referred to the web version of this article.)

of the microstructure. Similar observation is reported by Sangid et al. [13] for the nano-twinned Ni–Co alloys of different compositions. Enhanced damage properties in the presence of nano-sized twins in pure Cu have also been experimentally observed by Singh et al. [12]. Most recently, other researchers have also undertaken both experimental and modeling endeavors to cast light on the mechanistic origin of the cracking behavior in nano-twinned microstructure [6,45]. In the current work, utilizing the concept of near-tip slip irreversibility, we forward a theory to explain the currently observed experimental trends as well as those in the literature. In doing so, we consider the crack-emitted slip interacting with CTBs, leading to most reversible cyclic slip.

It is well established in the earlier literature that the near-threshold fatigue crack growth is microstructure-sensitive, and is decided by the nature of near-tip slip and slip–barrier interactions [46,47]. For the current nanotwinned Ni–Co alloys in question, the central role of CTBs would be manifested in the form of their unique capability of allowing either easy slip transfer or obstruct the glide. The specific outcome of slip–CTB reaction is reportedly dependent on the local stress state (i.e. on the incident, boundary and outgoing slip systems), and the associated slip geometry [20]. Recent findings by Chowdhury et al. [16,21] suggest that an increasing magnitude of residual slip, b_r, at the twin boundary can be correlated with enhanced irreversible slip as triggered by a differential of forward and reverse plastic flow at the interface. Increased irreversibilities due to the flow differential would inevitably elevate crack growth rate in near threshold regime. In this regard, the cross-slip phenomenon is likely to incur the most reversible slip trajectory during a fatigue cycle, due principally to the absence of any b_r (hence, no flow differential) at the boundary [16,19]. In the early literature, the phenomenon of cross-slipping at the CTB has been addressed quite extensively using molecular dynamics framework [48,49]. We have built on these foundations laid by the earlier researchers in applying to the current fatigue problem.

The very absence of b_r for cross-slip case removes the forward and reverse flow differential during the fatigue cycle, and hence renders the glide path more reversible. Given the present experimental observations of superior fatigue crack growth resistance in presence of nanotwins, the theoretical study of cross-slip on fatigue resistances is justified. On the theoretical grounds (at both atomistic and continuum levels), we have predicted fatigue crack growth metrics based the CTB-induced cross-glide, and the results compare well with the experimental behavior of the nanotwinned Ni–Co alloys. With the current theory, we identify the role of three particular parameters that would readily affect the crack growth resistance: (1) the frictional stress $\sigma_F^{\text{Barrier}}$, (2) twin nano-dimensions (i.e. lamellar thickness, t, and inter-twin spacing, s) and, (3) the pre-existent dislocation density in the near-tip zone. We discuss the individual contribution of these factors as follows.

The strength of CTBs in obstructing dislocation glide $\sigma_F^{\text{Barrier}}$ is mainly determined by the geometry of slip–twin interaction mechanism and can also depend on alloy composition [35]. The trends in Fig. 9 show the enhancement of fatigue damage impedance as a result of various values of $\sigma_F^{\text{Barrier}}$ for the cross-slip case. With increasing values of $\sigma_F^{\text{Barrier}}$, the dislocation motion is obstructed

by a greater extent. The obstruction of crack-emitted slip influences the degree of the cyclic slip irreversibility, which in turn controls the incremental crack extension. To illustrate how increasing $\sigma_F^{\text{Barrier}}$ influences the irreversibility, let us consider a hypothetical case of a boundary with very large $\sigma_F^{\text{Barrier}}$, at which slip is completely obstructed. In such case, the crack-emitted slip remains in the close vicinity of the advancing crack, and can easily glide back towards the crack during the load reversal. This situation would lead to a highly reversible slip motion. In other words, in case of no flow stress differential (i.e. for cross-slip case), the gradually increasing $\sigma_F^{\text{Barrier}}$ (which represent both forward and reverse flow strength) would impart a greater fatigue crack growth resistance.

In addition to the CTB strength $\sigma_F^{\text{Barrier}}$, we observe that there also exists a beneficial effect of the reduced twin dimensions (i.e. lamellar thickness and inter-twin spacing) on the damage resistance of nanotwinned alloys. The $\Delta K_{\text{eff}}^{\text{th}}$ level demonstrably improves with decreasing thickness/spacing. With the current dislocation simulations, we have shown the mechanistic origin of such effect in terms of the increasing density of twin boundaries in front of the advancing crack. For instance, within a certain distance from the crack-tip, refinement in the twin thickness/spacing essentially results in an increased number of boundaries, to be encountered by the crack-emitted slip. As a result, the degree of overall dislocation obstruction would be greatly enhanced i.e. the prevalence of slip-barriers creates increased shielding against the near-tip plastic flow. A reduced extent of crack-tip plasticity would in turn incur lower slip irreversibility. Since the incremental crack extension is directly proportional to the slip irreversibility, the crack growth is therefore significantly suppressed. This effect is reflected in terms of a substantial enhancement of the $\Delta K_{\text{eff}}^{\text{th}}$ levels with decreasing twin thickness/spacing.

The initial dislocation density in the near-tip region is another crucial factor, which decides the crack growth resistance. From the current simulations, the role of pre-existent near-tip dislocation is observed to be governed by the sign of the Burgers' vector. If the initial dislocations have the same sign as the crack-emitted slip, the repulsive forces between them would suppress the very emission process. Due to the suppression of crack-induced slip emanation, the overall cyclic slip trajectory becomes more reversible. This effect is quantified in the form of enhanced $\Delta K_{\text{eff}}^{\text{th}}$ with increasing initial dislocation numbers, n^C (in Fig. 11). The role of prior dislocations of opposite sign is insignificant since they are eventually annihilated with the crack-emitted ones, thereby posing no shielding effects.

In summary, the examination of experimental data for Ni–Co 600 HT (Fig. 2) has indicated that ΔK_{eff} spans a larger spectrum of values in near threshold regime unlike Ni–Co. With the current simulation results, we show that the spatial variation of t or s values on the crack path has considerable influence on the crack growth behavior. The predicted values under an average t, s and initial dislocation density values (highlighted as red, yellow, blue and green) are compared side by side for Ni–Co and Ni–Co 600 HT. Since the as-received Ni–Co was not subjected to twin coarsening heat treatment, its homogeneous microstructure distribution bounds ΔK_{eff} in a constant slope zone. As opposed to this trend, Ni–Co 600 HT shows a transition in the slope because of various distributions of twin thickness/spacing values due to heat treatment. That is why, in our modeling considerations, we have utilized the average thickness/spacing to predict the experimental behavior.

The primary contribution of the current theory is to predict the crack growth resistance for the case of cross-gliding of crack-emitted slip at a CTB (leaving zero residual slip, b_r). Such consideration is particularly important, in that the cross-slip results in the maximum reversibility of the slip trajectory. Chowdhury et al. [16] demonstrated that the slip transfer mechanism with non-zero b_r generates a flow strength differential for forward and reverse glide. As pointed out earlier, the existence of such flow differential promotes cyclic slip irreversibility, which in turn is proportional to the crack growth rate. In that regard, the currently considered cross-slip case, having zero b_r, is the most important slip–CTB interaction mechanism, leading to the greatest crack propagation impedance. The predicted values of the damage tolerance metrics (expressed in terms of $\Delta K_{\text{eff}}^{\text{th}}$) manifestly supports the present assumption. Moreover, we have particularly identified the most pertinent microstructural variables, namely, twin thickness/spacing, prior dislocation presence and barrier strength. Exploring the roles of individual parameters on the predicted $\Delta K_{\text{eff}}^{\text{th}}$ levels provides important mechanistic understanding of how to achieve optimized microstructure for maximum damage tolerance.

6. Conclusions

In this study, we have analyzed the fatigue crack growth behavior of nanotwinned Ni–2.89 wt.% Co both experimentally and theoretically. Tailoring the twin thickness and spacing by heat treatment enabled to unveil the effects thereof on the fatigue damage resistance. To pinpoint the physical mechanisms governing the crack advancement, dislocation motion simulations were conducted as informed by the underlying atomistic parameters. The current work reveals the following:

(1) From experiments, the high volume fraction of twins is observed to impart enhanced fatigue damage impedance. The improved damage resistance can be directly associated with a reduced degree of the measured irreversible strain levels at the crack tip. These findings pave the way for the further exploration of the physics of microstructure-sensitive crack propagation theoretically.
(2) Given the high damage resistance as determined experimentally, the crack-emitted slip–twin boundary interaction corresponding to the maximum reversibility i.e. the cross-slip case is studied in molecular dynamics simulations. Particularly, energy barrier to cross-glide is quantified, and fed into Peierls–Nabarro formulations in order to extract the corresponding friction stress. The predicted friction stresses constitute an essential ingredient in formulating a comprehensive fatigue crack growth model so that we can assess the critical role of the nano-twins on the cyclic damage behavior.
(3) The most important revelations obtained from the dislocation based fatigue simulations concern the quantification of the damage resistance (in terms of $\Delta K_{\text{eff}}^{\text{th}}$) subjected to the variations in: (i) the frictional stress levels, (ii) pre-existent near-tip slip, and (iii) the twin lamellar thickness and spacing. These findings are unprecedented and conform to the current experimental observations as well as those in the literature.
(4) The most important contribution of the current work can be deemed as forwarding a physically based model to assess the century-old empirical fatigue problem. Particularly, we have demonstrated what necessary parameters and/or tools from the existing literature could be utilized to solve the fatigue problem, which also bears future potential for expansion.

Acknowledgements

The support of Honeywell Aerospace Corporation is gratefully acknowledged. We also acknowledge the use of Taub cluster, the parallel computing resource, at the University of Illinois.

Appendix A

In presence of a dislocation, the atomic registry across the slip plane deviates from the equilibrium configuration. The nature of disregistry of a dislocation is based on the local displacement distribution as given in Eq. (A.1) [50].

$$f(ma' - u^*) = b_{\text{par}} + \frac{b_{\text{par}}}{\pi}\left[\tan^{-1}\left(\frac{ma' - u^* - \frac{1}{2}w(u^*)}{\xi}\right) + \tan^{-1}\left(\frac{ma' - u^* + \frac{1}{2}w(u^*)}{\xi}\right)\right] \tag{A.1}$$

In the disregistry function expression, $f(ma' - u^*)$, a' is the lattice periodicity in Burgers' vector direction of the partial dislocations and is equal to $2d/\sqrt{6}$ for face centered cubic lattice structure [16]. b_{par} is the magnitude of a partial dislocation given by $|1/6\,[1\,1\,2]|$. m index represents the discrete lattice structure and it can range from $+\infty$ to $-\infty$ depending on the convergence. It ranges from 0 to $2b$ which is the magnitude of the each partial dislocation forming the full screw dislocation. ξ is the dislocation core half width, $x_c/2$, and w is the separation distance between leading and trailing partials as a function of u^* collected from the MD simulation data. The misfit energy can be calculated by Eq. (A.2). Note that γ_{us} for cross-glide case is evaluated as 362 mJ/m^2 whereas it is 305 mJ/m^2 for the unobstructed glide. The expressions for the elastic energy, E^{elastic}, and the work done, W, can be seen in Eqs. (A.3) and (A.4). R is the crystal dimension and taken as 500 times of ξ.

$$E^{\text{misfit}}(u^*) = \sum_{m=-\infty}^{m=+\infty} \gamma(f(ma' - u^*))a' \tag{A.2}$$

$$E^{\text{elastic}} = \frac{Gb^2}{4\pi}\ln\frac{R}{\xi} \tag{A.3}$$

$$W = \sigma_F b \tag{A.4}$$

One of the essential ingredients of predicting σ_F and/or $\sigma_F^{\text{Barrier}}$ within PN formalism is the fault energy profile (i.e. the so-called γ surface), which traditionally been treated as a mere sinusoidal curve on an ad hoc basis. As a result, an exponential expression for Peierls (friction) stresses [40,41,50] has been proposed in the previous literature. Moreover, the traditional PN stress formulation does not have any provision for an input to predict the extrinsic levels of friction stress (e.g. under the influence of local stress). Thus, it is important that the friction stresses be solved numerically within the fundamental PN premise as outlined above, which would be the most accurate strategy to obtain the CTB-influenced stresses. To that end, one requires the precise shape/size of the γ surface. As a result, one is able to correctly capture the inherent material resistance to slip in the form of discrete lattice energetics.

References

[1] Lu L, Chen X, Huang X, Lu K. Revealing the maximum strength in nanotwinned copper. Science 2009;323:607–10.
[2] Yuan F, Chen P, Wu X. Tensile deformation mechanisms of the hierarchical structure consisting of both twin-free grains and nanotwinned grains. Philos Mag Lett 2014;94:514–21.
[3] Lu K, Yan FK, Wang HT, Tao NR. Strengthening austenitic steels by using nanotwinned austenitic grains. Scr Mater 2012;66:878–83.
[4] Pan QS, Lu QH, Lu L. Fatigue behavior of columnar-grained Cu with preferentially oriented nano scale twins. Acta Mater 2013;61:1383–93.
[5] Shute CJ, Myers BD, Xie S, Barbee TW, Hodge AM, Weertman JR. Microstructural stability during cyclic loading of multilayer copper/copper samples with nanoscale twinning. Scr Mater 2009;60:1073–7.
[6] Kim S-W, Li X, Gao H, Kumar S. In situ observations of crack arrest and bridging by nanoscale twins in copper thin films. Acta Mater 2012;60:2959–72.
[7] Chowdhury P, Sehitoglu H, Abuzaid W, Maier H. Mechanical response of low stacking fault energy Co–Ni alloys – continuum, mesoscopic and atomic level treatments. Int J Plast 2015;71:32–61.
[8] Antolovich SD, Armstrong RW. Plastic strain localization in metals: origins and consequences. Prog Mater Sci 2014;59:1–160.
[9] McDowell DL. A perspective on trends in multiscale plasticity. Int J Plast 2010;26:1280–309.
[10] Horton JA, Ohr SM. TEM observations of the motion of crack tip produced dislocations during cyclic loading in aluminum. Scr Metall 1982;16:621–6.
[11] Guo XL, Lu L, Li SX. Dislocation evolution in twins of cyclically deformed copper. Philos Mag Lett 2005;85:613–23.
[12] Singh A, Tang L, Dao M, Lu L, Suresh S. Fracture toughness and fatigue crack growth characteristics of nanotwinned copper. Acta Mater 2011;59:2437–46.
[13] Sangid MD, Pataky GJ, Sehitoglu H, Rateick RG, Niendorf T, Maier HJ. Superior fatigue crack growth resistance, irreversibility, and fatigue crack growth-microstructure relationship of nanocrystalline alloys. Acta Mater 2011;59:7340–55.
[14] Wu XJ, Koul AK, Krausz AS. A transgranular fatigue crack growth model based on restricted slip reversibility. MTA 1993;24:1373–80.
[15] Sangid MD, Ezaz T, Sehitoglu H. Energetics of residual dislocations associated with slip–twin and slip–GBs interactions. Mater Sci Eng A – Struct Mater Prop Microstruct Process 2012;542:21–30.
[16] Chowdhury PB, Sehitoglu H, Rateick RG. Predicting fatigue resistance of nanotwinned materials: Part I – role of cyclic slip irreversibility and Peierls stress. Int J Fatigue 2014;68:277–91.
[17] Ezaz T, Sangid MD, Sehitoglu H. Energy barriers associated with slip–twin interactions. Phil Mag 2011;91:1464–88.
[18] Zhu YT, Wu XL, Liao XZ, Narayan J, Kecskes LJ, Mathaudhu SN. Dislocation–twin interactions in nanocrystalline fcc metals. Acta Mater 2011;59:812–21.
[19] Sutton AP, Balluffi RW. Interfaces in crystalline materials. New York: Oxford Science Publications; 1996.
[20] Lee TC, Robertson IM, Birnbaum HK. Prediction of slip transfer mechanisms across grain boundaries. Scr Metall 1989;23:799–803.
[21] Chowdhury PB, Sehitoglu H, Rateick RG. Predicting fatigue resistance of nanotwinned materials: Part II – Effective threshold stress intensity factor range. Int J Fatigue 2014;68:292–301.
[22] Chowdhury PB, Sehitoglu H, Rateick RG, Maier HJ. Modeling fatigue crack growth resistance of nanocrystalline alloys. Acta Mater 2013;61:2531–47.
[23] Pippan R. Dislocation emission and fatigue crack growth threshold. Acta Metall Mater 1991;39:255–62.
[24] Pippan R. The condition for the cyclic plastic deformation of the crack type – the influence of dislocation obstacles. Int J Fract 1992;58:305–18.
[25] Peierls R. The size of a dislocation. Proc Phys Soc 1940;52:34–7.
[26] Nabarro FRN. Dislocations in a simple cubic lattice. Proc Phys Soc 1947;59:256–72.
[27] NiCoForm Incorporation. <http://www.nicoform.com/files/upload/upload/23/Mechanical.pdf>; 7 July 2015.
[28] Plimpton S. Fast parallel algorithms for short-range molecular dynamics. J Comput Phys 1995;117:1–19.
[29] Zhou XW, Johnson RA, Wadley HNG. Misfit-energy-increasing dislocations in vapor-deposited CoFe/NiFe multilayers. Phys Rev B 2004;69:1–10.
[30] Chowdhury P. Fatigue crack growth (FCG) modeling in the presence of nano-obstacles. Urbana-Champaign: University of Illinois; 2011.
[31] Humphrey W, Dalke A, Schulten K. VMD: visual molecular dynamics. J Mol Graph 1996;14:33–8.
[32] Li J. AtomEye: an efficient atomistic configuration viewer. Modell Simul Mater Sci Eng 2003;11:173–7.
[33] Suresh S. Fatigue of materials. 2nd ed. New York: Cambridge University Press; 2001.
[34] Hertzberg R. Deformation and fracture mechanics of engineering materials. John Wiley & Sons; 1976.
[35] Chowdhury P, Sehitoglu H, Maier HJ, Rateick R. Strength prediction in NiCo alloys – the role of composition and nanotwins. Int J Plast 2013.
[36] Rice JR, Thomson R. Ductile versus brittle behavior of crystals. Phil Mag 1974;29:73–97.
[37] Ohr SM. An electron microscope study of crack tip deformation and its impact on the dislocation theory of fracture. Mater Sci Eng 1985;72:1–35.
[38] Vitek V. Intrinsic stacking faults in body centered cubic crystals. Phil Mag 1968;18:773–86.
[39] Majumdar BS, Burns SJ. Crack tip shielding – an elastic theory of dislocations and dislocations arrays near a sharp crack. Acta Metall 1981;29:579–88.
[40] Joos B, Ren Q, Duesbery MS. Peierls–Nabarro model of dislocations in silicon with generalized stacking fault restoring forces. Phys Rev B 1994;50:5890–8.
[41] Hirth JP, Lothe J. Theory of dislocations. New York: John Wiley & Sons; 1982.
[42] Eshelby JD. The force on an elastic singularity, philosophical transactions of the royal society of London. Ser A, Math Phys Sci 1951;244:87–112.
[43] Vitek V, Yamaguchi M. Core structure of nonscrew 1/2 (1 1 1) dislocations on (1 1 0) planes in b.c.c. crystals. II. Peierls stress and the effect of an external shear stress on the cores. J Phys F: Met Phys 1973;3:537–42.

[44] Riemelmoser FO, Pippan R. Investigation of a growing fatigue crack by means of a discrete dislocation model. Mater Sci Eng A – Struct Mater Prop Microstruct Process 1997;234:135–7.
[45] Zeng Z, Li X, Lu L, Zhu T. Fracture in a thin film of nanotwinned copper. Acta Mater 2015;98:313–7.
[46] Miller KJ. Materials science perspective of metal fatigue resistance. Mater Sci Technol 1993;9:453–62.
[47] Hornbogen E, Gahr K-HZ. Microstructure and fatigue crack growth in a γ-Fe–Ni–Al alloy. Acta Metall 1976;24:581–92.
[48] Jin Z-H, Gumbsch P, Ma E, Albe K, Lu K, Hahn H, et al. The interaction mechanism of screw dislocations with coherent twin boundaries in different face-centred cubic metals. Scr Mater 2006;54:1163–8.
[49] Zhu T, Li J, Samanta A, Kim HG, Suresh S. Interfacial plasticity governs strain rate sensitivity and ductility in nanostructured metals. Proc Natl Acad Sci 2007;104:3031–6.
[50] Schoeck G. The generalized Peierls–Nabarro model. Philos Mag A – Phys Condens Matter Struct Defect Mech Prop 1994;69:1085–95.